Biomaterials 82 (2016) 168–177

Contents lists available at ScienceDirect

Biomaterials

journal homepage: www.elsevier.com/locate/biomaterials

# Cell source determines the immunological impact of biomimetic nanoparticles

Michael Evangelopoulos [a, 1], Alessandro Parodi [a, b, 1], Jonathan O. Martinez [a], Iman K. Yazdi [a], Armando Cevenini [a, c, d], Anne L. van de Ven [a], Nicoletta Quattrocchi [a], Christian Boada [a, e], Nima Taghipour [a], Claudia Corbo [a], Brandon S. Brown [a], Shilpa Scaria [a], Xuewu Liu [a], Mauro Ferrari [a], Ennio Tasciotti [a, *]

[a] Department of Nanomedicine, Houston Methodist Research Institute, Houston, TX 77030, USA
[b] Department of Experimental Oncology and Molecular Medicine, Fondazione IRCCS Istituto Nazionale Tumori, Milan 20133, Italy
[c] Department of Molecular Medicine and Medical Biotechnology, University of Naples "Federico II", Via Pansini 5, 80131 Naples, Italy
[d] CEINGE-Biotecnologie Avanzate s.c.a.r.l., Via Gaetano Salvatore 486, 80145 Naples, Italy
[e] Escuela de Medicina y Ciencias de la Salud, Tecnologico de Monterrey, Monterrey, Nuevo Leon, Mexico

ARTICLE INFO

*Article history:*
Received 12 October 2015
Received in revised form
17 November 2015
Accepted 28 November 2015
Available online 2 December 2015

*Keywords:*
Drug delivery
Multistage nanovector
Immunobiology
Nanoparticles
Leukolike Vector
Biomimicry

ABSTRACT

Recently, engineering the surface of nanotherapeutics with biologics to provide them with superior biocompatibility and targeting towards pathological tissues has gained significant popularity. Although the functionalization of drug delivery vectors with cellular materials has been shown to provide synthetic particles with unique biological properties, these approaches may have undesirable immunological repercussions upon systemic administration. Herein, we comparatively analyzed unmodified multistage nanovectors and particles functionalized with murine and human leukocyte cellular membrane, dubbed Leukolike Vectors (LLV), and the immunological effects that may arise *in vitro* and *in vivo*. Previously, LLV demonstrated an avoidance of opsonization and phagocytosis, in addition to superior targeting of inflammation and prolonged circulation. In this work, we performed a comprehensive evaluation of the importance of the source of cellular membrane in increasing their systemic tolerance and minimizing an inflammatory response. Time-lapse microscopy revealed LLV developed using a cellular coating derived from a murine (i.e., syngeneic) source resulted in an active avoidance of uptake by macrophage cells. Additionally, LLV composed of a murine membrane were found to have decreased uptake in the liver with no significant effect on hepatic function. As biomimicry continues to develop, this work demonstrates the necessity to consider the source of biological material in the development of future drug delivery carriers.



## 1. Introduction

Recent discoveries have demonstrated that biomimicry can be employed to bestow synthetic carriers with surface modifications derived from biological components, thereby providing robust physiological tolerances and biological targeting [1–3]. In particular, our group previously demonstrated cellular membranes of circulating leukocytes could be easily isolated and transferred onto the surface of synthetic nanocarriers while maintaining key biological functions. These carriers, referred to as Leukolike Vectors (LLV) [4], are composed of a loadable [5], biodegradable [6,7], and biocompatible [8,9] multistage nanovector (MSV) [10–13] core with a proteolipid outer shell purified from leukocyte cell membrane (CM). This outer layer was shown to retain membrane proteins [14] that are critical for increased adhesion towards inflamed endothelium [15] while also providing prolonged circulation time [16].

With the recent popularity of biomimetic delivery platforms, the evaluation of carrier biocompatibility continues to remain a major component for the successful translation into the clinic. Nevertheless, current literature lacks a comprehensive analysis on

* Corresponding author. Department of Nanomedicine, Houston Methodist Research Institute, 6670 Bertner Ave., MS R10-316, Houston, TX 77030, USA.
*E-mail address:* etasciotti@tmhs.org (E. Tasciotti).
[1] These authors contributed equally.

http://dx.doi.org/10.1016/j.biomaterials.2015.11.054

the biological impact of these new drug delivery platforms; in particular, systemic and cellular inflammation, as well as the toxicity of isolated CM applied onto synthetic carriers are unknown, regardless of various efforts to understand the working mechanism of immune cells and their clinical potential. More so, despite various sources demonstrating the clinical potential of syngeneic (i.e., genetically compatible) leukocyte treatments for cancer, little is known of the potential side effects a xenogeneic (i.e., genetically incompatible) model may yield. In addition, a comparative analysis of the potential side effects that can be caused by syngeneic and xenogeneic membranes applied to a synthetic nanocarrier have not previously been investigated. Herein, we performed a comprehensive study of the biological impact the source of membrane (i.e., murine and human) has when applied to MSV and compared to uncoated particles, both *in vitro* and *in vivo*. Our findings indicate the source of membrane is critical in inhibiting cellular internalization and rapid clearance of the particles *in vitro* and *in vivo*, respectively, although less so in triggering an acute inflammatory response.

## 2. Materials and methods

### 2.1. Fabrication of Leukolike Vectors

MSV were fabricated as previously described using published protocols [12]. Briefly, hemispherical 3.2 μm MSV with 15 nm pores were washed in isopropyl alcohol (IPA). Oxidation of MSV was performed by incubating particles in a 3:1 ratio of concentrated sulfuric acid to 30% hydrogen peroxide. Reaction was allowed to occur for 2 h with gradual heat being applied to bring the final temperature of the mixture to 90 °C. Following heating, solution was allowed to cool and MilliQ water was added to bring the concentration of sulfuric acid to 10% and allowed to cool for an additional 60 min with brief agitation. Particles were collected, centrifuged at 4500 × *g*, and washed three times with water. Next, particles were washed three times in IPA and used as needed. Amination of the surface with (3-aminopropyl)triethoxysilane (APTES, Sigma) was performed by suspending particles in a 2% APTES solution in IPA and incubated at 35 °C while mixing at 1300 RPM. Next, aminated particles were dried under vacuum overnight to polymerize the silane layer. Following polymerization, particles were washed three times in IPA and fluorescence-modification was performed by incubating APTES-conjugated particles with 1 mg $mL^{-1}$ Alexa Fluor 555 NHS Ester (Life Technologies) resuspended in dimethyl sulfoxide for 2 h at room temperature under brief mixing.

Fabrication of LLV was performed following previously established protocols [4]. Briefly, cellular membrane was extracted following brief homogenization of cells in homogenization buffer (250 mM sucrose, 10 mM Tris/HCl, 1 mM $MgCl_2$, 1 mM KCl, 2 mM phenylmethylsulfonyl fluoride, trypsin–chymotrypsin inhibitor 200 μg $mL^{-1}$, DNase 10 μg $mL^{-1}$, RNase 10 μg $mL^{-1}$; Sigma–Aldrich). Following homogenization, lysed celled were carefully layered onto a discontinuous sucrose gradient and centrifuged at 28,000 × *g* for 30 min at 4 °C. Plasma membrane was then collected and added to a 150 mM sodium chloride solution. Next, MSV particles were conjugated with (3-aminopropyl)triethoxysilane (APTES, Sigma) and, where stated, Alexa Fluor dyes (Invitrogen) as previously described [17]. Particles were then incubated with the proteolipid (i.e., Jurkat or J774 cell membrane extract) solution overnight at 4 °C under continuous rotation. Following incubation, particles were centrifuged at 200 × *g* for 10 min and washed twice in 150 mM NaCl. Assessment of particle surface charge was achieved by suspending 1 × $10^6$ particles into phosphate buffer (pH 7.4) solution and read using a Malvern ZetaSizer NanoZS. Unless otherwise stated, experiments using MSV particles were previously functionalized with APTES.

### 2.2. Time-lapse microscopy

The day before imaging, 2 × $10^4$ J774 cells were seeded into a 4-chamber slide (LabTek). DyLight 488-conjugated MSV, mLLV (containing PE-FITC) and hLLV (containing PE-Rhod) were used. Particles were added at a particle:cell ratio of 1.5:1. TLM was performed at HMRI Advanced Cellular and Tissue Microscope Core Facility using a Spinning Disk Confocal microscope (Olympus) equipped with an incubation chamber that maintained imaging conditions at 37 °C and 5% $CO_2$. Post-image analysis was performed by acquiring images every 3 min or 5 min using a 40× objective for 2 h. At each imaging point the DIC, FITC, and TRITC channels were collected and analyzed with Slidebook software to generate movies. Each movie was counted for free, associated, and internalized particles based on their proximity to the membranes of macrophages. The number of particles in each condition was counted at 15, 30, 60, 90, 120, and 150 min as well as the number of cells in the field of view. The percentage of particles was calculated by capping the maximum number of particles (i.e., 100%) at 150 min and normalizing previous time points to this condition.

### 2.3. Western blot

For the analysis of NF-κB activation and autophagy, 3 × $10^5$ J774 cells $well^{-1}$ were seeded into a 6 well plate. Following overnight incubation, cell samples were treated with complete media containing MSV (APTES), mLLV, hLLV, and LPS (1 μg $mL^{-1}$, Sigma) (as positive control for NF-κB activation) in 2 mL $well^{-1}$. Untreated cells represented the negative control. For the analysis of NF-κB activation, the cells were harvested 1.5 h after treatment to obtain nuclear or whole cell extracts and 24 h for autophagy. Cell extracts containing nuclear soluble proteins and cytosolic proteins were obtained using the Qproteome Nuclear Protein Kit (Qiagen) while whole cell extracts were obtained using a RIPA buffer (Thermo) with 1 μL Halt protease inhibitor cocktail (Thermo) per 100 mL of buffer. 40 μg of whole cell extract, 20 μg of cytosolic extract, or 10 μg of nuclear extract were loaded onto SDS-PAGE and transferred to a PVDF membrane for Western blot analysis. For the analysis of NF-κB activation, blots were incubated with the following primary antibodies: anti-NF-κB p65 (1:200 dilution), anti-TBP (1:2000 dilution), anti-β-actin (1:2000 dilution) (Santa Cruz Biotechnology). For the analysis of autophagy, blots were incubated with the following primary antibodies: anti-LC3 (1:2000 dilution) and anti-GAPDH (1:20,000 dilution). Following this incubation, membranes were then incubated with horseradish peroxidase (HRP)-conjugated secondary antibodies. Bands were visualized using a SuperSignal West Dura Chemiluminescent Substrate (Thermo) and images were acquired with ChemiDoc XRS+ System and Image Lab software (Bio-Rad). Quantitative analysis of the bands was performed using ImageJ software (NIH).

### 2.4. Cytokine and plasma analysis

For the analysis of cytokines levels *in vitro*, J774 cells were seeded at 5 × $10^4$ cells $well^{-1}$ into a tissue-culture treated 96-well plate and incubated overnight. Following incubation, cells were treated with oxidized and APTES-modified MSV, mLLV, hLLV, and zymosan (100 μg $mL^{-1}$, positive control) in complete media. Untreated cells represented a negative control. After 3 h and 24 h of treatment, media from each sample was collected and centrifuged at 10,000 × *g*. The supernatant was then collected and analyzed for

IL-1β, IL-6, IL-10, IL-12 p40, IL-12 p70, and TNF-α using the MILLIPLEX MAP Mouse Cytokine/Chemokine premixed Immunoassay plate (Millipore).

Cytokines, hepatic, and renal function for *in vivo* experiments were evaluated by collecting blood from treated BALB/c mice (n = 3) and evaluated for cytokines as mentioned using a MILLIPLEX MAP Mouse Cytokine/Chemokine premixed Immunoassay plate (Millipore). Hepatic and renal function was evaluated by evaluating blood serum for AST/ALT using an ALT Colorimetric Activity Assay and AST Colorimetric Activity Assay (Sigma). Creatinine levels were evaluated using a Creatinine Assay Kit (Abcam).

### 2.5. Intravital microscopy (IVM)

Live, wild-type BALB/c mice (Charles River) were imaged on an upright Nikon A1R laser scanning confocal microscope adapted for IVM [18]. Mice were anesthetized with isoflorane, surgically prepared to expose the left lobe of the liver [19], and injected intravenously with a 40 kDa FITC-dextran tracer (1 μM, Invitrogen) to delineate the vasculature [20]. Three days prior to imaging, mice received a one-time intravenous injection of DiD-labeled autologous red blood cells (RBCs, ~3% hematocrit) [21]. High-resolution time-lapse images of particle accumulation in the liver were acquired across multiple field-of-views (FOVs) for up to 2 h at 10–30 s intervals (30 fps) following a one-time intravenous injection of $0.5 \times 10^8$ particles in 50 μl PBS [19]. Particle accumulation dynamics were quantified frame-by-frame using NIS Elements v4.1 [19]. Particle biodistribution was assessed 1 h after particle injection, at which time the tissues harvested, sliced using a vibratome (Leica VT-1000), and imaged using the IVM system. The cumulative particle density for each organ was quantified using at least 200 randomly selected field-of-views (sized 4 mm × 4 mm × 3 μm) using NIS Elements v4.1 [21]. All animal protocols were reviewed and approved by the IACUC at Houston Methodist Research Institute.

### 2.6. Histology

Tissue samples were obtained from wild-type BALB/c mice (n = 3) that were subjected to a one-time injection of $10^8$ particles. Organ samples were collected from liver, spleen, and lung at day 2 and day 7 for each variable group. Organs were placed in formalin for 24 h before being transferred to a solution of 70% isopropyl alcohol and then imbedded with formalin (10%). Next, sections were deparafinnized using xylene, rehydrated with decreasing concentrations of alcohol, washed in water and stained with hematoxylin/eosin.

### 2.7. Statistical analysis

All results were collected and analyzed in triplicate and represented as a mean ± SD unless otherwise stated. All statistics were calculated using Prism GraphPad software. NF-κB and LC3 statistics were calculated using a student T-test. Cytokine expression, biodistribution, and *in vivo* cytokines were analyzed using a two-way analysis of variance (ANOVA) followed by a Bonferroni post-test comparing replicates means by rows.

## 3. Results and discussion

### 3.1. Synthesis and assembly of Leukolike Vectors

The synthesis of syngeneic (i.e., murine J774 macrophages, mLLV) and xenogeneic (i.e., human Jurkat T lymphocytes, hLLV) LLV was performed based on previously established techniques [4] for both *in vitro* and *in vivo* experiments. Briefly, leukocytes were collected, treated with an isotonic solution, and homogenized. Following centrifugation by layering lysed cells on a discontinuous sucrose gradient, plasma membrane was recovered and washed several times in a sodium chloride solution to remove nucleic fragments [22]. The adjoining of purified membranes onto the MSV surface was driven via electrostatic interactions between positively charged (3-aminopropyl)triethoxysilane (APTES)-modified MSV and negatively charged proteolipid membranes. Zeta potential measurements revealed APTES-conjugation of oxidized MSV resulted in a shift from −30.5 mV to +8.53 mV [6,7]. Functionalization with murine-derived CM (mCM) resulted in a drop of −18.44 mV from APTES MSV (+8.53 mV) to mLLV (−9.91 mV), approaching values consistent with intact leukocyte cells (−20.56 mV) (Fig. 1a). A similar shift in values was observed for LLV designed with human-derived CM (Fig. S1). Confirmation of a uniformly coated particle was assessed through scanning electron microscopy (SEM) demonstrating the complete coverage of the MSV pores following LLV assembly (Fig. 1b). Successful glycoprotein retention and protein orientation was evaluated using a wheat germ agglutinin immunofluorescence staining, specific to N-acetylglycosamine and sialic acid commonly found in proteins on the cells surface (Fig. 1c). The intensity profile of the coating was assessed by comparing the fluorescent signal of the CM to the MSV core, revealing an overlap of the CM (red) with the particles modified with fluorescein isothiocyanate (green) (Fig. 1d), validating the successful grafting of CM proteins onto the MSV surface and confirming previously published results [4]. Finally, western blot analysis of the LLV coating revealed the presence of critical leukocyte markers for self-tolerance (i.e., CD45, CD47, MHC-1, Fig. 1e). This data aligns with previously published results [4,14] and confirms the reproducibility of our assembly method as well as the presence of multiple leukocyte surface biomarkers in the proper orientation on the surface of MSV, including proteins that determine leukocyte biocompatibility and self-recognition.

### 3.2. Particle–macrophage interactions

The membrane coating was shown to be effective in inhibiting particle internalization, however, whether this phenomenon was an active inhibition of macrophage function or a cellular response mediated by the surface contact with the particles was not previously demonstrated. Through time-lapse microscopy experiments, we investigated the dynamics of this phenomenon by incubating J774 macrophages with MSV (Supplemental movie 1), mLLV (Supplemental movie 2), and hLLV (Supplemental movie 3) for 150 min at a ratio of 1.5:1 (particle:cell), in addition to macrophage co-treated with mLLV and hLLV (Supplemental movie 4). An initial analysis demonstrated J774 cells continuously patrol the surrounding environment for materials to internalize and detect surrounding particulates through surface interactions. Specifically, the cells demonstrated interactions with all particle groups; however, MSV and hLLV resulted with a firm interaction with the cells while mLLV maintained an unstable interaction that often resulted in the release of the particle following contact with the cell. This phenomenon is clearly shown in Supplementary movies 1–3 and snapshots depicted in Fig. 2a and Fig. S2. Quantitative analysis of free and associated/internalized particles was performed by evaluating representative sections of videos obtained through live microscopy and assessed for particle interaction with cells. Specifically, the fraction of free and interacting particles was manually counted at 15, 30, 60, 90, 120, and 150 min with the maximum particle percentage being obtained at 150 min (sufficient time to allow all particles to settle) and, as expected, the percentage

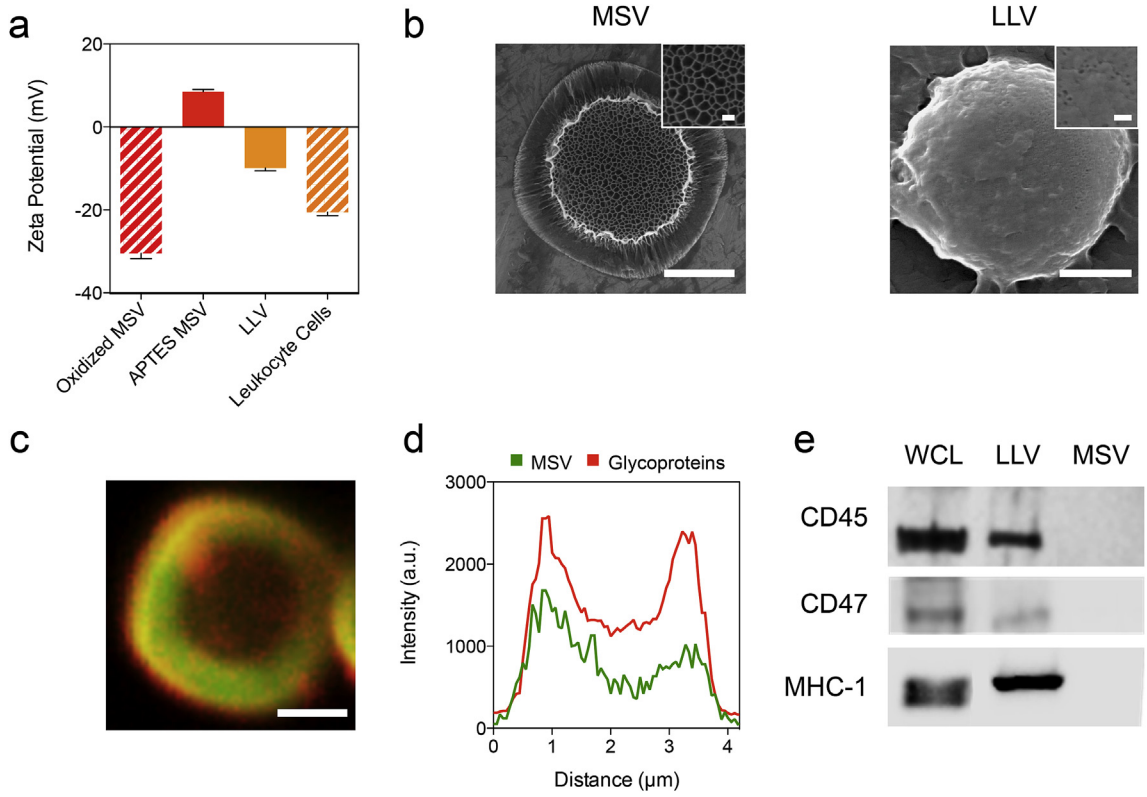


**Fig. 1.** Synthesis and assembly of Leukolike Vectors. (a) Bar graph comparing surface charge of particles before coating, after coating, and cells used to derive coating. (b) Scanning electron micrographs of MSV before coating and after coating with cellular membrane with high magnification insets showing change in pore visibility, scale = 1 μm, insets = 100 nm. (c) Confocal microscope image of particle (green) stained for WGA (red), scale = 1 μm. (d) Intensity plot of confocal image representing uniform distribution of WGA across particle. (e) Western blot analysis showing the presence of self-recognition proteins for whole cell lysate (WCL), LLV, and MSV. The data is plotted as a mean ± SD. (For interpretation of the references to colour in this figure legend, the reader is referred to the web version of this article.)

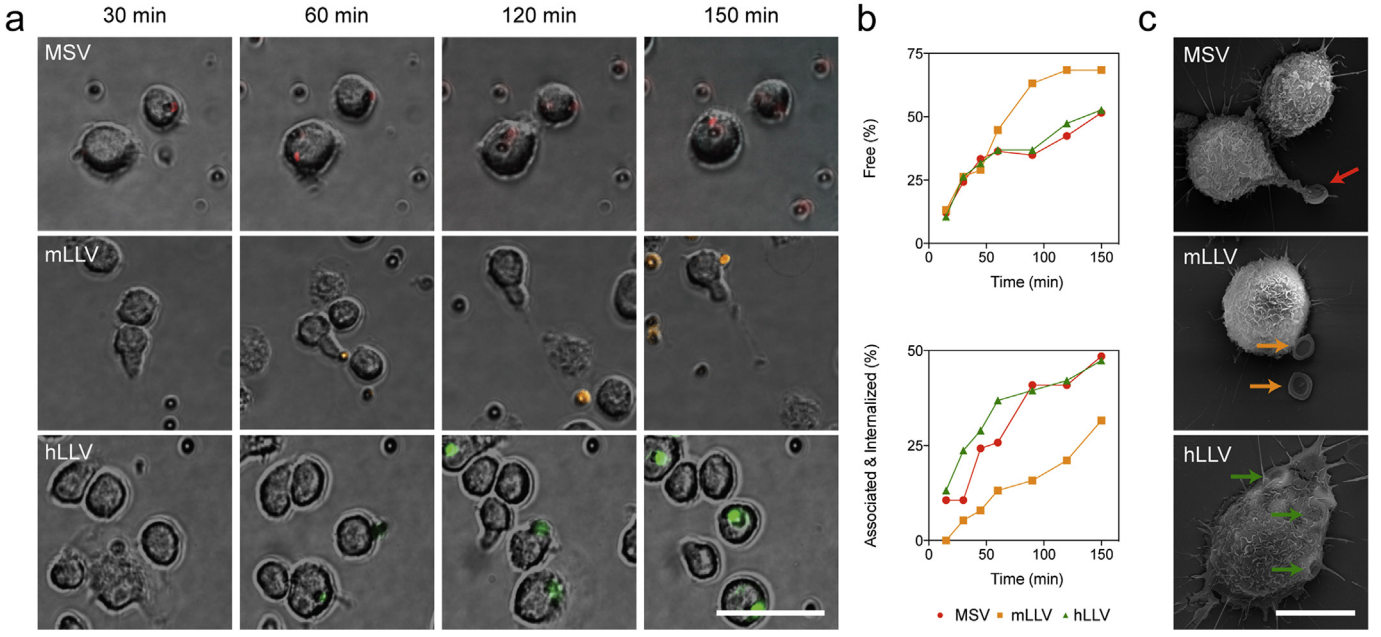


**Fig. 2.** Interaction of macrophage with MSV and LLV coated with murine and human-derived cell membranes. (a) Time lapse images of J774 cells treated with MSV (red), mLLV (orange), and hLLV (green) after 30, 60, 120, and 150 min, scale = 20 μm. (b) Selected positions from time-lapse microscopy were carefully analyzed to distinguish free and associated/internalized particles; one position was used for analysis for MSV, mLLV, and hLLV. (c) Scanning electron micrograph images of J774 cells after a 3 h treatment with MSV, mLLV, and hLLV. Visible particles depicted by arrows, scale = 10 μm. (For interpretation of the references to colour in this figure legend, the reader is referred to the web version of this article.)

of free mLLV was higher than MSV and hLLV (Fig. 2b). This phenomenon was further validated with flow cytometry and confocal microscopy, demonstrating mLLV resulted in a significant decrease in cell internalization (Fig. S3). Deeper investigation performed with SEM exhibited 3 h following treatment, macrophages exposed with MSV and hLLV resulted in the formation of filopodia-like structures, followed by particle internalization. Meanwhile, the same interactions with mLLV resulted in a simple docking of the particles on the cell surface (Fig. 2c). This data demonstrates the presence of a surface coating does not change the overall interaction with the cell, but can affect the internalization process.

Supplementary video related to this article can be found at http://dx.doi.org/10.1016/j.biomaterials.2015.11.054.

### 3.3. Cellular response upon treatment with LLV

The membrane coating applied on the particle surface may have the potential to trigger a cellular response following macrophage internalization ranging from inflammation, stress, and autophagocytosis. In order to test this hypothesis, macrophages were treated with unmodified MSV, mLLV, and hLLV at a 1:5 cell to particle ratio. The release of IL-6 and TNF-α, cytokines critical in the propagation of the inflammatory cascade [23], was measured after 3 and 24 h following treatment with zymosan, a molecule used to induce inflammation [24], being employed as a positive control. In all treatments, particles failed to trigger a significant release of IL-6 or TNF-α at both 3 h and 24 h compared to untreated macrophages while zymosan (i.e., positive control) displayed a significant elevation in both cytokines and at both time points (Fig. 3a). This data indicates that neither the core, nor the source of the membrane coating, was effective in increasing the level of inflammatory biomarkers *in vitro*.

Additionally, macrophage interaction with foreign particulates typically occurs through toll-like receptors whose signaling activate the NF-kB pathway (i.e., effect on cellular stress [25,26], response to reactive oxygen species [27] and foreign stimuli), thus activating the transcription of cytokine/chemokine genes and other pro-inflammatory pathways. Hence, to further evaluate the effect of the source of membrane, we evaluated NF-kB activation following a 90 min treatment with particles using previously established protocols. Western blot analysis was used to detect the nuclear levels of the p65/RelA subunit of NF-κB, typical assay performed to detect the activation of this biomarker (Fig. 3b) [28]. MSV, mLLV, and hLLV did not induce any significant variation in the p65/RelA protein expression, indicating that the contribution of a cellular coating to MSV did not result in the activation of the NF-κB pathway. However, when treated with a positive control (i.e., lipopolysaccharide, LPS), a significant increase in NF-κB expression resulted, indicating the source of the CM is not sufficient in triggering stress events. Furthermore, toll-like receptor signaling has also been shown to induce autophagy [29] and, more recently, nanoparticles with unique physiochemical characteristics have emerged as autophagy-inducers [30]. To investigate the onset of autophagy in macrophages, we assessed the ratio of LC3-I to LC3-II, a common indicator of autophagy [29,31,32], through western blot analysis following a 24 h treatment with particles (Fig. 3c). In this case, all treatment groups were found to express significantly elevated ratios of LC3-I/LC3-II compared to untreated groups, however, no significant difference was observed when compared to MSV. Furthermore, although elevated levels of autophagy were witnessed among the treatment groups, no significant variations were observed for particles with a proteolipid shell, indicating that mLLV and hLLV maintain similar safety in regards to MSV as previously reported [6,9].

### 3.4. Sequestration in MPS organs and biodistribution in vivo

Next, to evaluate the importance of the membrane source in preventing sequestration by the mononuclear phagocyte system (MPS) *in vivo*, we evaluated the accumulation kinetics of the particles in the primary filtration organ of the MPS (i.e., liver). Our results demonstrate that by measuring the real-time hepatic accumulation over a period of 90 min using intravital microscopy [4,17,33], a delay in particle hepatic accumulation was observed for mLLV. BALB/c mice (i.e., strain from which J774 cells were purified) were administered a one-time co-injection of MSV/mLLV or MSV/hLLV (Fig. 4). Both MSV and hLLV demonstrated rapid accumulation in the liver following a logarithmic trend that plateaued at approximately 5 min (Fig. 4a). On the other hand, mLLV displayed delayed accumulation in the liver with sigmoidal characteristics reaching comparable hepatic accumulation after more than 1 h. The effect of a syngeneic CM coating in delaying particle clearance from the circulation was further confirmed by evaluating biodistribution in major MPS organs *ex vivo* using confocal microscopy (Fig. 4b). For all particles tested, the spleen, lung, and liver represented the major organs of accumulation, with minor accumulation detected in the kidneys. More so, deposition of MSV and hLLV was found to be similar for all organs with no significance between the two while mLLV exhibited a significant decrease in lung accumulation and significantly higher blood circulation. Particle accumulation ratios (i.e., liver:spleen:lung:blood) exhibited advantageous values for mLLV at 1:4:1:1 compared to the higher values for MPS organs for MSV and hLLV at 7:17:10:1 and 10:21:12:1, respectively. Surprisingly, xenogeneic and mLLV displayed uniform distribution at the liver as determined by longitudinal and transverse sectioning, however, morphological differences were observed at the cellular level. Specifically, internalized hLLV were predominately clustered at the Kupffer cell centers, whereas mLLV were more widely spaced and predominately found at the Kupffer cell periphery (Fig. 4c). This data provides further insight into the membrane's potential to delay sequestration of MSV and the importance of the membrane source in delaying liver accumulation and prolonging circulation. Additionally, this confirms previous results obtained *in vitro* and demonstrates the coating derived from a syngeneic source was not only effective in increasing the circulation time of the particles but it also reduced the overall accumulation of the particles in the lungs.

### 3.5. Pathological implications in vivo

Next, the impact of membrane source on the MPS organ ultrastructure was evaluated 2 and 7 days following particle administration by examining hematoxylin and eosin stained tissues sections from BALB/c mice (i.e., strain from which J774 cells were purified). For pathological evaluation, a higher dose of particles was injected ($1 \times 10^8$ particles mouse$^{-1}$) compared to typical particle administration [34] in an effort to exacerbate the potential for an acute response. At 2 d, symptoms of increased pulmonary cellularity and cell packing density were apparent for all treatments compared to the untreated control (Fig. 5A). This effect was more evident in lower magnification images revealing an effect extended to the overall lung parenchyma (Fig. S4). Additionally, a substantial amount of particles were found in the liver with cells displaying empty cytoplasms, in addition to the formation of lymphatic centers (yellow dotted box). In spleen, no indication of stress was apparent in any of the treatments despite particles being readily visible at higher magnifications (yellow arrows). This data exhibits the lung as the principal organ to experience an adverse effect, with no considerable difference between the different treatments.

Notably, 7 d following administration, lung thickness of the

alveolar parenchyma was comparable to control mice demonstrating reduced organ cellularity when compared to day 2 and more evident in mLLV (Fig. 5B). Additionally, the liver and spleen of treated groups displayed a return to normal cell morphology and a decrease in particle retention, suggesting particle clearance or degradation. These results reveal the side effects on organ ultrastructure are mitigated by the system's ability to clear the particles and/or degrade them. Furthermore, mLLV demonstrated superior biocompatibility as witnessed by the reduced thickness of the alveolar septa. To better understand the CM contribution to the observed effects, a greater amount of CM than was used to coat the particles was injected and organs were observed at 2 and 7 d. Similar to the results obtained from MSV and LLV injections, an increase in the thickness of the alveolar septa in the lungs was

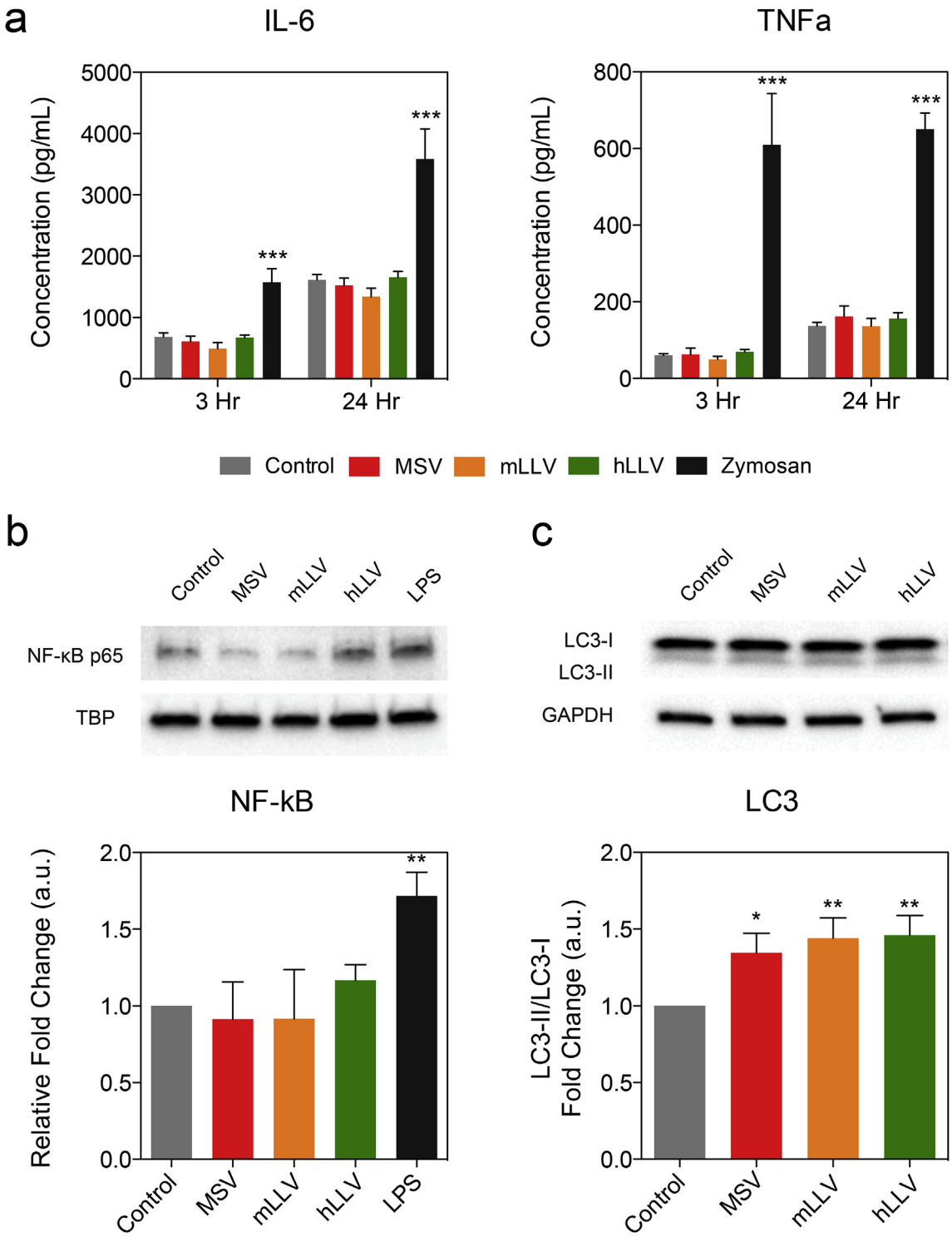


**Fig. 3.** Cytokine expression and autophagy. (a) Cytokine expression 3 and 24 h following administration of particles. (b) Western blot analysis of NF-κB p65 nuclear levels and (c) LC3-I/LC3-II 3 h after particle administration and quantification of NF-κB expression relative to TATA-binding protein. The data is plotted as a mean ± SD. *p < 0.05; ***p < 0.001.

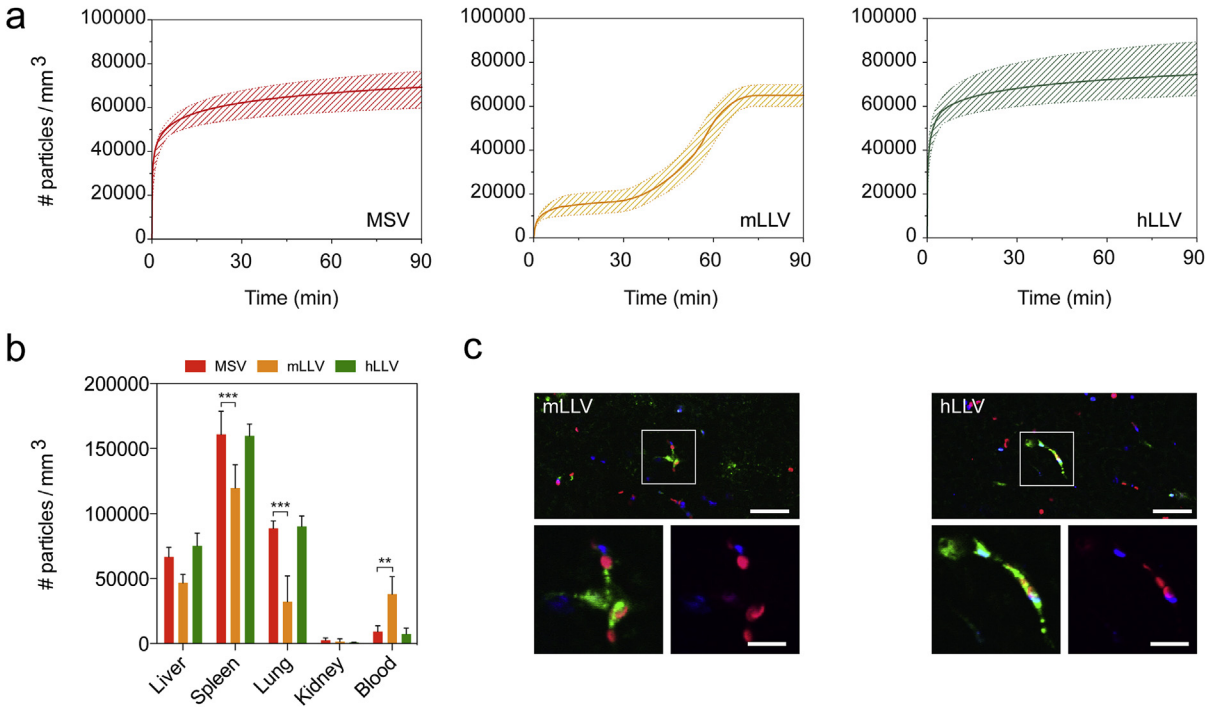


**Fig. 4.** Sequestration of particles *in vivo*. (a) Time dependent accumulation of particles MSV, mLLV, and hLLV in liver of BALB/c mice measured using intravital microscopy. Data is plotted as a mean curve ±1 SD. (b) Intravital data of particle distribution in organs harvested 60 min following injection, $^{**}p < 0.01$, $^{***}p < 0.001$. (c) Distribution of MSV (blue) in liver 90 min following simultaneous injection with mLLV or hLLV (red), (scale, 25 μm). High magnification images demonstrate internalization of particles at Kupffer cell centers (green), scale = 10 μm. (For interpretation of the references to colour in this figure legend, the reader is referred to the web version of this article.)

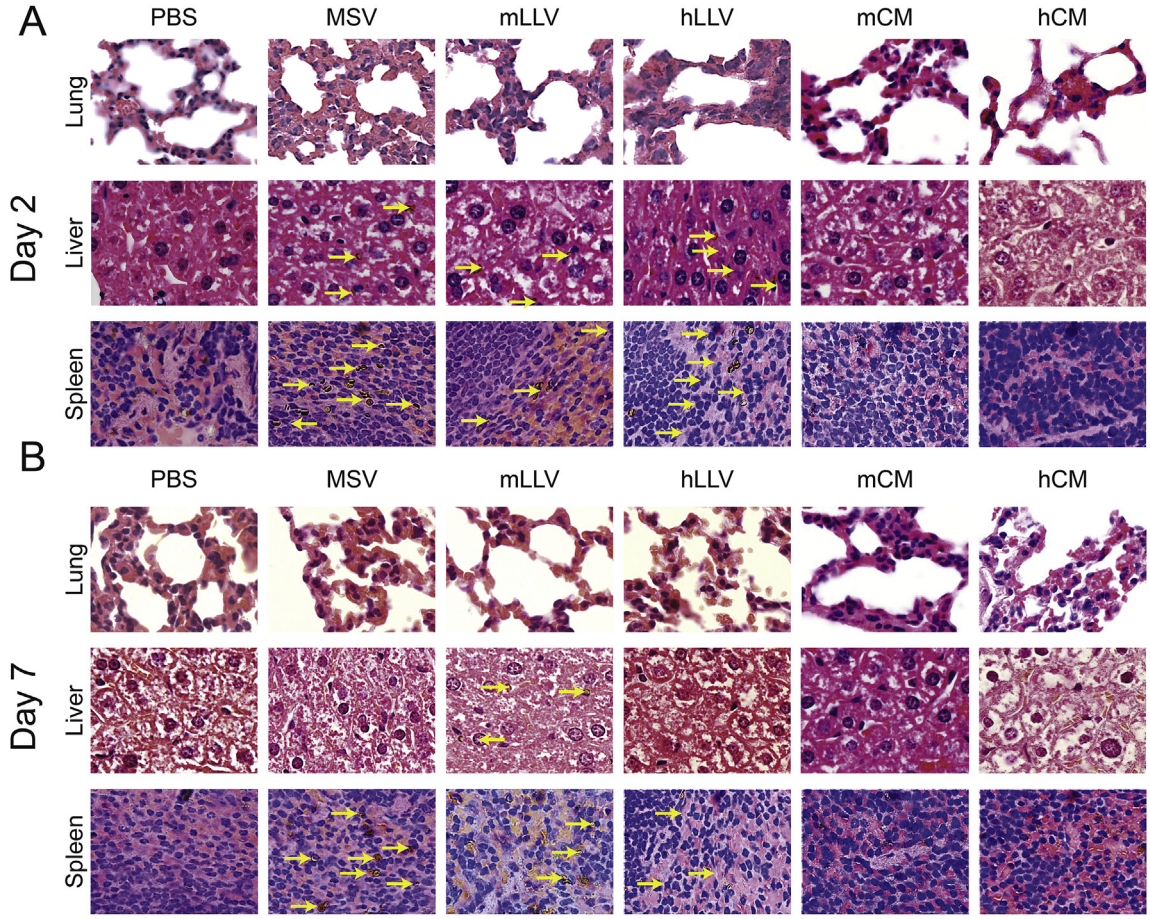


**Fig. 5.** Histological analysis. (A) Representative histological images of lung, liver, and spleen 2 days and (B) 7 days after treatment. Particles depicted by yellow arrows. (For interpretation of the references to colour in this figure legend, the reader is referred to the web version of this article.)

observed for both membrane sources. This included a visible impact on the morphology of the cell cytoplasm, with a more apparent effect for human-derived membrane (Fig. 4). Remarkably, murine-derived membranes appeared to have no evident effect on the liver while human-derived membranes displayed hepatocytes with empty cytoplasm, indicating signs of stress. Additionally, no long-term signs of stress were observed on the spleen with symptoms displaying a transient effect that diminished after one week, indicating a return to normal organ function. This data is critical in demonstrating the potential effects the membrane source can pose on organs of the MPS. Through pathological evaluation, we demonstrate, for the first time, that the addition of a membrane coating on MSV results in a minimal acute response and has a more pronounced effect only when the membrane source is derived from a xenogeneic source. This data also provides further insight into the membrane's potential to delay the sequestration of MSV and the importance of the membrane source in delaying liver accumulation and prolonging circulation. Additionally, this confirms previous results obtained *in vitro* and demonstrates the coating derived from a syngeneic source was not only effective in increasing the circulation time of the particles but also reducing the overall accumulation in the lungs. Lastly, this data demonstrates the addition of a proteolipid shell on the MSV results in comparable pathological effects on major MPS organs as uncoated MSV.

### 3.6. Cytokine expression in vivo and systemic toxicity

To evaluate the inflammatory implications of our system *in vivo*, the blood of BALB/c mice was collected following treatment and assessed for the presence of circulating soluble cytokines and biomarkers specific for hepatic and renal function. Specifically, a panel of ten cytokines was evaluated at 2 and 7 days following treatment with particles and compared to the levels obtained 2 h following LPS (i.e., positive control) administration. Interestingly, only interferon gamma (IFNγ), IL-2, and IL-3 displayed elevated cytokine levels (Fig. 6) while IL-1α, IL-1β, IL-6, IL-10, IL-12, KC and TNF-α all displayed significantly lower values for particle treatments compared to LPS (Fig. S5). Furthermore, initial values for IFNγ were elevated for coated particles (i.e., syngeneic and xenogeneic) and CM when compared to LPS, though 7 d following treatment, values were consistent with untreated mice. Correspondingly, levels of IL-2 and IL-3 were slightly elevated for particle groups, displaying a statistically significant difference among CM treatments, although expression did not exceed that of LPS and matched untreated groups at 7 d. This data demonstrates that while an initial immunological response is observed for mLLV and hLLV, cytokine levels return to healthy values one week following administration, indicating a transient effect on cytokine expression. Additionally, an evaluation of the aspartate transaminase–alanine transaminase ratio revealed no significant differences following mLLV administration at both 2 and 7 d, while hLLV displayed a significant decrease compared to untreated controls, indicative of liver dysfunction (Fig. 6d). Similarly, an assessment of creatinine levels, an important indicator in renal function, revealed no significant difference between mLLV and untreated groups, while hLLV displayed a significant decrease in creatinine levels even one week

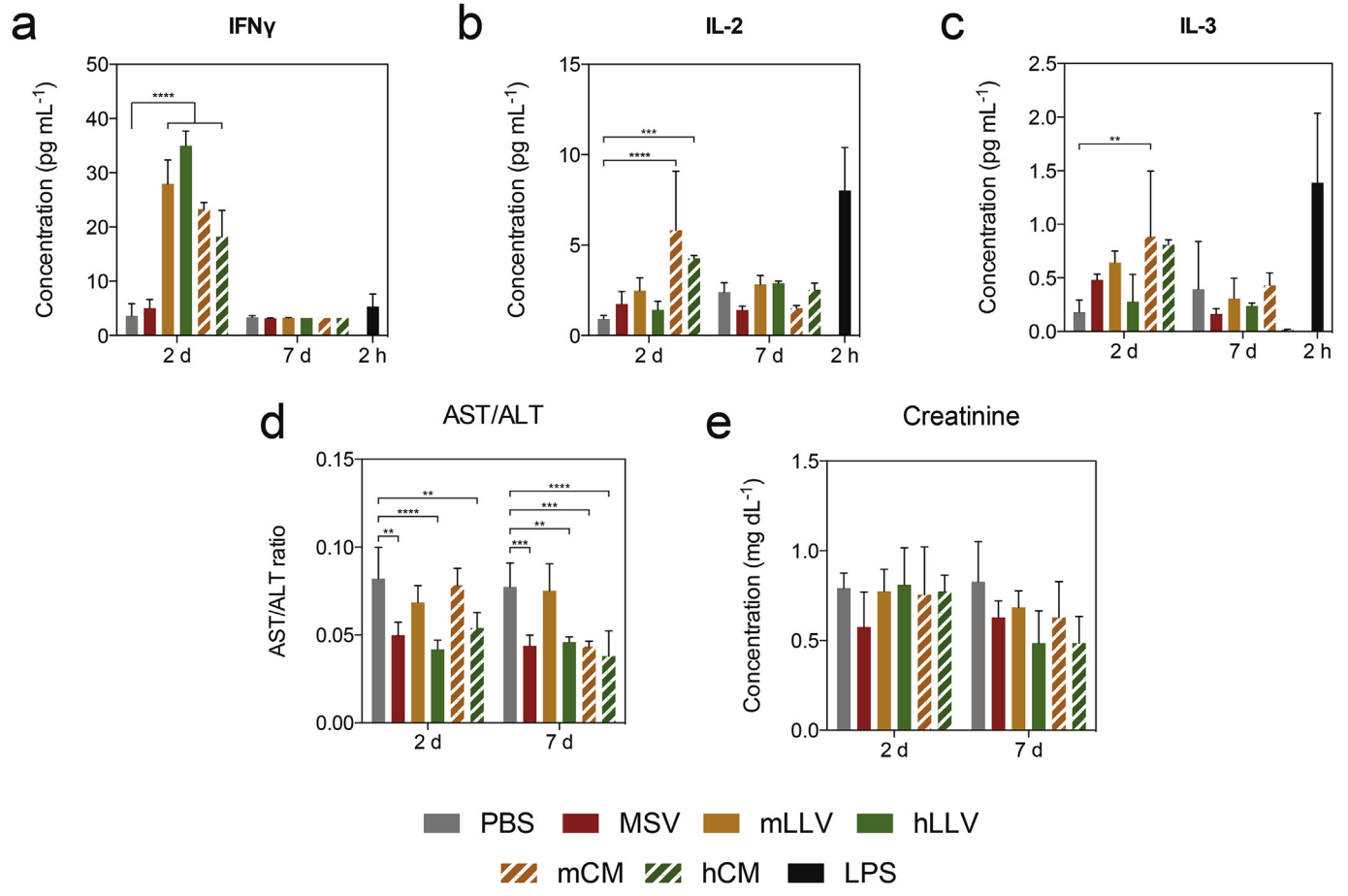


**Fig. 6.** Evaluation of plasmatic levels of cytokines and hepatic biomarkers of stress. Cytokine levels expressed in blood of BALB/c mice were evaluated for (a) IFNγ, (b) IL-2, (c) IL-3, (d) AST/ALT and (e) creatinine, 2 and 7 days following treatment with positive control, LPS shown at 2 h. The data is plotted as mean ± SD. *p < 0.05, **p < 0.01, ***p < 0.001.

after particle administration (Fig. 6e). This demonstrates a favorable response when the membrane source is derived from a syngeneic source and exhibits undesirable characteristics for xenogeneic material, particularly related to renal function.

## 4. Conclusion

Collectively, these findings suggest that mLLV was most effective in delaying uptake by macrophages *in vitro*, likely due to the presence of critical biomarkers and self-recognition receptors preserved within the cellular coating. Additionally, the presence of a membrane coating was not sufficient in raising the expression of inflammatory cytokines *in vitro* when compared to MSV and did not induce autophagy. Notably, *in vivo* results demonstrated mLLV resulted in prolonged circulation and delayed sequestration by the liver, providing favorable delivery vector kinetics. An analysis of critical MPS organs revealed all particle groups impacted the ultrastructure of the organs at day 2 with xenogeneic CM inducing the most substantial effects, particularly to the lung and liver. This effect on the organ ultrastructure was largely attributed to the presence of both an MSV core and a membrane coating, however, ultrastructure damage and particle accumulation greatly diminished one week following treatment, consistent with previous reports [9]. Interestingly, cytokines involved in the activation of T lymphocytes (i.e., IFNγ, IL-2, IL-3) were found to be elevated 2 d post treatment, though levels returned to healthy values at 7 d. This initial cell-mediated immune response was likely due to an altered surface composition of the LLV compared to leukocytes. Notably, in this work we characterized, for the first time, the *in vitro* and *in vivo* impact of a biomimetic delivery systems assembled by coating a nanoporous vehicle with syngeneic- or xenogeneic-derived CM. Furthermore, this works highlights the importance of considering the membrane source in the development of bio-inspired nanomaterials. In fact, a syngeneic-derived coating displayed favorable properties in preventing internalization by the MPS *in vitro* and *in vivo*, as well as favorable biocompatibility in comparison to uncoated MSV and hLLV.

## Acknowledgments

The authors would like to thank Kemi Cui and HMRI Advanced Cellular and Tissue Microscope Core Facility for traditional confocal scanning services, David Haviland and the HMRI Flow Cytometry Core Facility for flow cytometry setup and acquisition, and Sarah Amra from Histopathology Services at The Brown Foundation Institute of Molecular Medicine, part of The University of Texas Health Science Center at Houston for assistance in histological preparation. This work was supported by the National Institute of Health (NIH) (1R21CA173579-01A1 and 5U54CA143837) with internal support provided by HMRI including the Cullen Trust for Health Care Foundation (Project ID: 18130014); A.P. acknowledges support from the Bianca Garavaglia Association (Busto Arsizio, Italy). M.F. is supported by the Ernest Cockrell Jr. Distinguished Endowed Chair.

## Appendix A. Supplementary data

Supplementary data related to this article can be found at http://dx.doi.org/10.1016/j.biomaterials.2015.11.054.

## References

[1] G. von Maltzahn, J.H. Park, K.Y. Lin, N. Singh, C. Schwoppe, R. Mesters, et al., Nanoparticles that communicate in vivo to amplify tumour targeting, Nat. Mater. 10 (2011) 545–552.
[2] T.J. Merkel, S.W. Jones, K.P. Herlihy, F.R. Kersey, A.R. Shields, M. Napier, et al., Using mechanobiological mimicry of red blood cells to extend circulation times of hydrogel microparticles, Proc. Natl. Acad. Sci. U. S. A. 108 (2011) 586–591.
[3] J.O. Martinez, M. Evangelopoulos, V. Karun, E. Shegog, J.A. Wang, C. Boada, et al., The effect of multistage nanovector targeting of VEGFR2 positive tumor endothelia on cell adhesion and local payload accumulation, Biomaterials 35 (2014) 9824–9832.
[4] A. Parodi, N. Quattrocchi, A.L. van de Ven, C. Chiappini, M. Evangelopoulos, J.O. Martinez, et al., Synthetic nanoparticles functionalized with biomimetic leukocyte membranes possess cell-like functions, Nat. Nanotechnol. 8 (2013) 61–68.
[5] J.O. Martinez, M. Evangelopoulos, R. Bhavane, S. Acciardo, F. Salvatore, X. Liu, et al., Multistage nanovectors enhance the delivery of free and encapsulated drugs, Curr. Drug Targets 16 (2015) 1582–1590.
[6] J.O. Martinez, M. Evangelopoulos, C. Chiappini, X. Liu, M. Ferrari, E. Tasciotti, Degradation and biocompatibility of multistage nanovectors in physiological systems, J. Biomed. Mater. Res. Part A 102 (2014) 3540–3549.
[7] J.O. Martinez, C. Chiappini, A. Ziemys, A.M. Faust, M. Kojic, X. Liu, et al., Engineering multi-stage nanovectors for controlled degradation and tunable release kinetics, Biomaterials 34 (2013) 8469–8477.
[8] J.O. Martinez, A. Parodi, X. Liu, M.G. Kolonin, M. Ferrari, E. Tasciotti, Evaluation of cell function upon nanovector internalization, Small 9 (2013) 1696–1702.
[9] J.O. Martinez, C. Boada, I.K. Yazdi, M. Evangelopoulos, B.S. Brown, X. Liu, et al., Short and long term, in vitro and in vivo correlations of cellular and tissue responses to mesoporous silicon nanovectors, Small 9 (2013) 1722–1733.
[10] E. Tasciotti, X. Liu, R. Bhavane, K. Plant, A.D. Leonard, B.K. Price, et al., Mesoporous silicon particles as a multistage delivery system for imaging and therapeutic applications, Nat. Nanotechnol. 3 (2008) 151–157.
[11] J.O. Martinez, B.S. Brown, N. Quattrocchi, M. Evangelopoulos, M. Ferrari, E. Tasciotti, Multifunctional to multistage delivery systems: the evolution of nanoparticles for biomedical applications, Chin. Sci. Bull. 57 (2012) 3961–3971.
[12] C. Chiappini, E. Tasciotti, J.R. Fakhoury, D. Fine, L. Pullan, Y.C. Wang, et al., Tailored porous silicon microparticles: fabrication and properties, Chemphyschem – Eur. J. Chem. Phys. Phys. Chem. 11 (2010) 1029–1035.
[13] J. Wolfram, H. Shen, M. Ferrari, Multistage vector (MSV) therapeutics, J. Control. Release 219 (2015) 406–415.
[14] C. Corbo, A. Parodi, M. Evangelopoulos, D.A. Engler, R.K. Matsunami, A.C. Engler, et al., Proteomic profiling of a biomimetic drug delivery platform, Curr. Drug Targets 16 (2015) 1540–1547.
[15] C. Ruegg, Leukocytes, inflammation, and angiogenesis in cancer: fatal attractions, J. Leukoc. Biol. 80 (2006) 682–684.
[16] P.A. Oldenborg, A. Zheleznyak, Y.F. Fang, C.F. Lagenaur, H.D. Gresham, F.P. Lindberg, Role of CD47 as a marker of self on red blood cells, Science 288 (2000) 2051–2054.
[17] A.L. van de Ven, P. Kim, O. Haley, J.R. Fakhoury, G. Adriani, J. Schmulen, et al., Rapid tumoritropic accumulation of systemically injected plateloid particles and their biodistribution, J. Control. Release – Off. J. Control. Release Soc. 158 (2012) 148–155.
[18] A.L. van de Ven, M. Wu, J. Lowengrub, S. McDougall, M.A. Chaplain, V. Cristini, et al., Integrated intravital microscopy and mathematical modeling to optimize nanotherapeutics delivery to tumors, AIP Adv. 2 (2012), 011208.
[19] A.L. van de Ven, P. Kim, M. Ferrari, S.H. Yun, Real-time intravital microscopy of individual nanoparticle dynamics in liver and tumors of live mice, Nat. Protoc. Exch. (2013), http://dx.doi.org/10.1038/protex.2013.049 , url: http://www.nature.com/protocolexchange/protocols/2706.
[20] A.L. van de Ven, B. Abdollahi, C.J. Martinez, L.P. Burey, M.D. Landis, J.C. Chang, et al., Modeling of nanotherapeutics delivery based on tumor perfusion, New J. Phys. 15 (2013), 055004.
[21] A.L. van de Ven, P. Kim, O. Haley, J. Fakhoury, G. Adriani, J. Schmulen, et al., Rapid tumoritropic accumulation of systemically injected plateloid particles and their biodistribution, J. Control. Release 158 (2012) 148–155.
[22] J. Sambrook, D.W. Russell, Removal of Small Fragments of Nucleic Acid from Preparations of Plasmid DNA by Centrifugation through NaCl, CSH Protoc. 2006 (2006).
[23] H. Roca, L.K. McCauley, Inflammation and skeletal metastasis, Bonekey Rep. 4 (2015) 706.
[24] J.L. Cash, G.E. White, D.R. Greaves, Zymosan-induced peritonitis as a simple experimental system for the study of inflammation (Chapter 17), Methods Enzym. 461 (2009) 379–396.
[25] A.R. Brasier, The NF-kappaB regulatory network, Cardiovasc. Toxicol. 6 (2006) 111–130.
[26] T. Wang, X. Zhang, J.J. Li, The role of NF-kappaB in the regulation of cell stress responses, Int. Immunopharmacol. 2 (2002) 1509–1520.
[27] A. Siomek, NF-kappaB signaling pathway and free radical impact, Acta Biochim. Pol. 59 (2012) 323–331.
[28] P.O. Gannon, L. Lessard, L.M. Stevens, V. Forest, L.R. Begin, S. Minner, et al., Large-scale independent validation of the nuclear factor-kappa B p65 prognostic biomarker in prostate cancer, Eur. J. Cancer 49 (2013) 2441–2448.
[29] M.A. Sanjuan, C.P. Dillon, S.W. Tait, S. Moshiach, F. Dorsey, S. Connell, et al., Toll-like receptor signalling in macrophages links the autophagy pathway to phagocytosis, Nature 450 (2007) 1253–1257.
[30] Y. Zhang, F. Zheng, T. Yang, W. Zhou, Y. Liu, N. Man, et al., Tuning the autophagy-inducing activity of lanthanide-based nanocrystals through

specific surface-coating peptides, Nat. Mater. 11 (2012) 817–826.
[31] I. Tanida, T. Ueno, E. Kominami, LC3 and autophagy, Methods Mol. Biol. 445 (2008) 77–88.
[32] A. Parodi, S.G. Haddix, N. Taghipour, S. Scaria, F. Taraballi, A. Cevenini, et al., Bromelain surface modification increases the diffusion of silica nanoparticles in the tumor extracellular matrix, ACS Nano 8 (2014) 9874–9883.
[33] A.L. van de Ven, P. Kim, M. Ferrari, S.H. Yun, Real-time Intravital Microscopy of Individual Nanoparticle Dynamics in Liver and Tumors of Live Mice, 2013.
[34] J. Shen, H.C. Kim, C. Mu, E. Gentile, J. Mai, J. Wolfram, et al., Multifunctional gold nanorods for siRNA gene silencing and photothermal therapy, Adv. Healthc. Mater. 3 (2014) 1629–1637.